

# Design and Implementation of Active Power Control with Improved P&O Method for Wind PV-Battery Based Standalone Generation System

Suman Kumar Rajak<sup>1</sup>, Ravi Kant Yadav<sup>2</sup>

**Abstract:** In this paper, the design and implementation of active power control (APC) with fuzzy controller and compared with anti-windup PI controller (AWPI) and improved perturbation and observation (P&O) method with sliding mode control (SMC), are researched to get abnormal state of execution with diminished number of sensors for a steady activity of a breeze PV-battery based cross breed independent power age framework (HSPGS). This paper presents the six cases of design and implementation of active power control with improved P & O method for wind PV-Battery based standalone generation system. The performance of APC based controller includes the wind or PV changes, steady state, sudden increased of load, unbalanced linear load and balanced- unbalanced non-linear load.

**Keywords:** Hybrid standalone power generation system (HSPGS), Wind turbine (WT), solar photovoltaic array (SPVA), sliding mode control (SMC), Perturbation and observation method (P & O), antiwindup PI controller (AWPI), fuzzy controller, active power control (APC)

## 1. Introduction

Several remote areas in the world use only diesel generators (DGs) to support their electricity needs. This energy source (ES) is costly and pollutant. However, hybrid standalone power generation system (HSPGS) based on wind and solar energy supported by the battery energy storage system (BESS) is considered as a promising solution for remote areas to reduce diesel-fuel dependency, to minimize the greenhouse (GHS) emissions, to reduce power transmission, and to minimize the system losses[1]. This new technology is effective however, it requires improvement especially in the design and control to become simple and easy to use.

Regarding, the efficiency of SPVA and WT, many methods are developed in the literature to track the maximum power point (MPP) [3, 4]. Compared to the existing MPP tracking (MPPT) methods, perturbation and observation (P&O) is extensively applied as an easy method.

### 1.1 Maximum Power Point Tracking

Maximum power point tracking is a technique used commonly with wind turbines and photovoltaic (PV) solar systems to maximize power extraction under all conditions. Albeit sun oriented power is predominantly secured, the guideline applies by and large to sources with variable power: for instance, optical power transmission and thermophotovoltaics. The control at the MPP" (Pmpp) is the" result of the MPP voltage (Vmpp) and MPP current (Impp)."

### 1.2 MPPT Methods

This paper compares 7 different methods along derivatives of two of the methods. These methods include:

- 1) Constant Voltage
- 2) Open Circuit Voltage
- 3) Short Circuit Current
- 4) Perturb and Observe
- 5) Incremental Conductance
- 6) Temperature
- 7) Temperature Parametric MPPT methods 1 through 5 are covered in this document.

### 1.3 Perturb and Observe

Perturb and Observe (P and O) searches for the maximum power point by changing the PV voltage or current and detecting the change in PV power output. "The course of the change is turned around when the PV power diminishes". P and O can have issues at low irradiance that result in oscillation. There can also be issues when there are fast changes in the irradiance which can result in initially choosing the wrong direction of search.

## 2. System Configuration

Fig.1 shows the proposed HSPGS configuration for isolated areas that possess a good wind and solar potential. It consists of SPVA, WT driven variable speed permanent magnet brushless DC generator (PMBLDCG), BESS, two boost converters, a three-phase diode rectifier, interfacing DC-AC power inverter, LC low-pass filter, loads, and a DC dump load. To avoid the synchronization issues, all DERs are connected to the DC bus. Three control strategies are developed to ensure stable and affective operation of HSPGS under sever conditions.

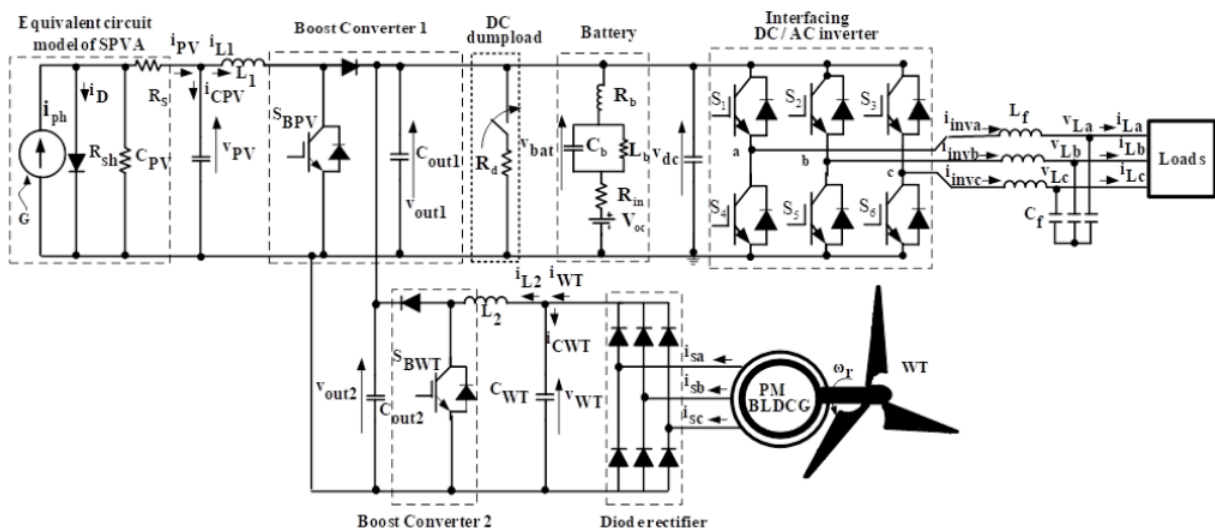


Figure 1: HSPGS configuration under study

### 3. Modeling and Control Strategies

In this section, modeling and developed control strategies for boost power converters of SPVA and WT, and an interfacing three-phase power inverter, as well as, the stability analysis, are given in detail.

#### A. Modeling and control design for SPVA :

From Fig.1, a boost converter of SPVA, is modeled as follows.

$$L_1 (\partial i_{L1} / \partial t) = v_{PV} \tag{1}$$

$$C_{out1} (\partial v_{out1} / \partial t) = -v_{out1} / R \tag{2}$$

$$i_{CPV} = C_{PV} (\partial v_{CPV} / \partial t) = i_{PV} - i_{L1} \tag{3}$$

And for  $S_{BPV}=0$  (OFF),

$$L_1 (\partial i_{L1} / \partial t) = v_{PV} - v_{out1} \tag{4}$$

$$C_{out1} (\partial v_{out1} / \partial t) = i_{L1} - (v_{out1} / R) \tag{5}$$

$$(\partial i_{PV} / \partial t) = \overbrace{(v_{PV} / L_1) - (1 - d_1)(v_{out1} / L_1)}^{Term1} + \overbrace{C_{PV} (\partial^2 v_{PV} / \partial t^2)}^{Term2} \tag{8}$$

where  $d_1$  is the desired control. The variation of the  $v_{PV}$  during court duration is equal to zero. However, the second

Where  $S_{BPV}$ ,  $L_1$ ,  $C_{PV}$ ,  $C_{out1}$ ,  $R$ ,  $i_{L1}$ ,  $i_{PV}$ ,  $i_{CPV}$ ,  $v_{out1}$ , and  $v_{CPV}$  represent the switch, inductance, input and output capacitances, equivalent load resistance, inductor current, output PV current, input capacitor current, output voltage, and input capacitor voltage of the boost converter1, respectively. Based on (1) to (5), the following equations for boost converter 1, are obtained as,

$$(\partial i_{L1} / \partial t) = (v_{PV} / L_1) - (1 - d_1)(v_{out1} / L_1) \tag{6}$$

$$(\partial v_{out1} / \partial t) = (1 / C_{out1}) [(i_{L1} (1 - d_1)) - (v_{out1} / R)] \tag{7}$$

Rearranging (6), one gets the following expression as,

$$(\partial i_{PV} / \partial t) = (v_{PV} / L_1) - (1 - d_1)(v_{out1} / L_1) \tag{9}$$

derivative of  $v_{PV}$  is equal to zero. Hence, expression given in (8) becomes as follows,

#### 1) Control strategy for the Boost converter-1

Fig.2 shows the control scheme of the improved P&O method based on SMC with boundary layer, which is used to achieve high performance from SPVA and to ensure the

stability during sudden change in solar insolation in finite time.

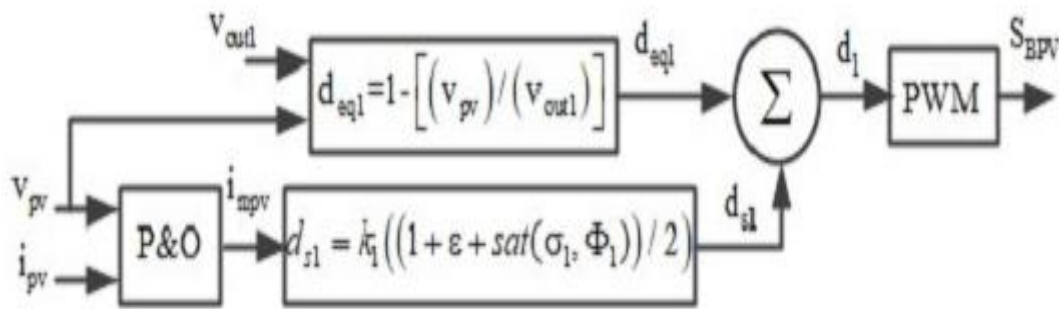


Figure 2: Improved P&O based SMC with boundary layer for SPVA

**B. Modeling and control design for WT**

As shown in Fig.1, stator terminals of PMBLDCG are connected to the DC bus through a diode rectifier and boost converter used to achieve the MPPT. Using this configuration, the WT voltage varies slightly with variation of the rotor speed, which makes possible to achieve MPPT without measuring rotor position or wind speed.

**1) Mathematical model of PMBLDCG**

The mathematical model of PMBLDCG is as follows [30],

$$[v_{sabc}] = R_s [i_{sabc}] + (L_s - M) [di_{sabc} / dt] + [e_{abc}] \tag{27}$$

where  $v_{sabc}$ ,  $i_{sabc}$ ,  $R_s$ ,  $L_s$ ,  $M$ ,  $e_{abc}$ , denote terminal voltages and currents, stator resistances, inductances, mutual inductance and the back-emf of PMBLDCG, respectively.

The electromagnetic torque of PMBLDCG, is described as,

$$T_e = (1 / \omega_r) (e_a i_{WTa} + e_b i_{WTb} + e_c i_{WTc}) \tag{28}$$

where  $\omega_r$  is the mechanical rotor speed and is defined as,

$$\omega_r = (2/P) \omega_e \tag{29}$$

where  $\omega_e$  and  $P$  denote the electrical frequency and the number of rotor poles, respectively.

The equation of motion of PMBLDCG is defined as,

$$T_m = T_e + J (d\omega_r / dt) + B\omega_r \tag{30}$$

Where  $J$ ,  $B$ ,  $T_m$  and  $T_e$  denote the moment of inertia, friction coefficient, developed torque and electromagnetic torque, respectively.

**2) Mathematical model of the boost converter-2**

From Fig.1, a boost converter of  $W_T$ , is modeled as follows. For,  $S_{BWT} = 1$  (ON),

$$L_2 (\partial i_{L2} / \partial t) = v_{WT} \tag{31}$$

$$C_{out2} (\partial v_{out2} / \partial t) = -v_{out2} / R \tag{32}$$

$$i_{CWT} = C_{WT} (\partial v_{CWT} / \partial t) = i_{WT} - i_{L2} \tag{33}$$

And for  $S_{BWT} = 0$  (OFF),

$$L_2 (\partial i_{L2} / \partial t) = v_{WT} - v_{out2} \tag{34}$$

$$C_{out2} (\partial v_{out2} / \partial t) = i_{WT} - (v_{out2} / R) \tag{35}$$

where  $S_{BWT}$ ,  $L_2$ ,  $C_{WT}$ ,  $C_{out2}$ ,  $R$ ,  $i_{L2}$ ,  $i_{WT}$ ,  $i_{CWT}$ ,  $v_{out2}$ , and  $v_{CWT}$  represent switch, inductance, input and output capacitances, equivalent load resistance, inductor current, output PV current, input capacitor current, output voltage, and input capacitor voltage of the boost converter-2, respectively. Based on (31) to (35), the following equations for boost converter-2, are obtained as,

$$(\partial (i_{WT} - i_{CWT}) / \partial t) = (\partial (i_{WT} - C_{WT} \partial v_{WT}) / \partial t) \tag{36}$$

$$= (v_{WT} / L_2) - (1 - d_2) (v_{out2} / L_2)$$

$$(\partial v_{out2} / \partial t) = (1 / C_{out2}) [(i_{WT} (1 - d_2)) - (v_{out2} / R)] \tag{37}$$

Rearranging (36), following expression is obtained,

$$(\partial i_{WT} / \partial t) = \overbrace{(v_{WT} / L_2) - (1 - d_2) (v_{out2} / L_2)}^{Term1} + \overbrace{C_{WT} (\partial^2 v_{WT} / \partial t^2)}^{Term2} \tag{38}$$

where  $d_2$  is the desired control.

The variation of the  $v_{WT}$  during this duration is equal to zero. However, the second derivative of  $V_{WT}$  is also equal to zero. Hence, (37) becomes as follows,

$$(\partial i_{WT} / \partial t) = (v_{WT} / L_2) - (1 - d_2) (v_{out2} / L_2) \tag{39}$$

**3) Control strategy for boost converter-2**

An improved P&O method based SMC with boundary layer, is presented in Fig.3, which is developed to achieve high performance from WT driven variable speed PMBLDCG without mechanical sensors. It is also used to ensure stability at the operating point in finite time, during sudden change in wind speed. For this method, only output ( $v_{out2}$ ) and input ( $v_{WT}$ ) DC voltages and the inductor current ( $i_{L2}$ ) which is equal to the output WT current ( $i_{WT}$ ), are sensed to obtain the desired control  $d_2$ .

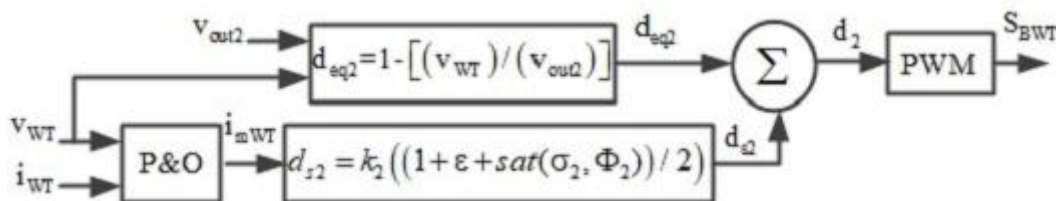


Figure 3: Improved P&O based SMC with boundary layer for WT

C. Modeling and control design of three-phase inverter

Fig.4 shows the control scheme of the APC based on AWPI controller for the AC voltage regulation. The system frequency is maintained constant by operating the DC-AC interfacing inverter at 60Hz. Applying Kirchoff’s voltage and current laws at the connection point of the three-phase interfacing inverter shown in Fig.1, following differential equations in natural three-phase coordinate system (a-b-c), are obtained as,

$$(di_{inv(abc)} / dt) = (1 / L_f)(d_{(abc)}V_{dc} - v_{L(abc)}) \tag{60}$$

$$(dv_{L(abc)} / dt) = (1 / C_f)(i_{inv(abc)} - i_{L(abc)}) \tag{61}$$

where  $d_{(abc)}$ ,  $v_{L(abc)}$ ,  $i_{inv(abc)}$ ,  $i_{L(abc)}$ ,  $V_{dc}$ ,  $C_f$  and  $L_f$  represent the control variable, AC voltages, output inverter currents, load currents, DC link voltage, capacitance and inductance of the inverter output filter, respectively.

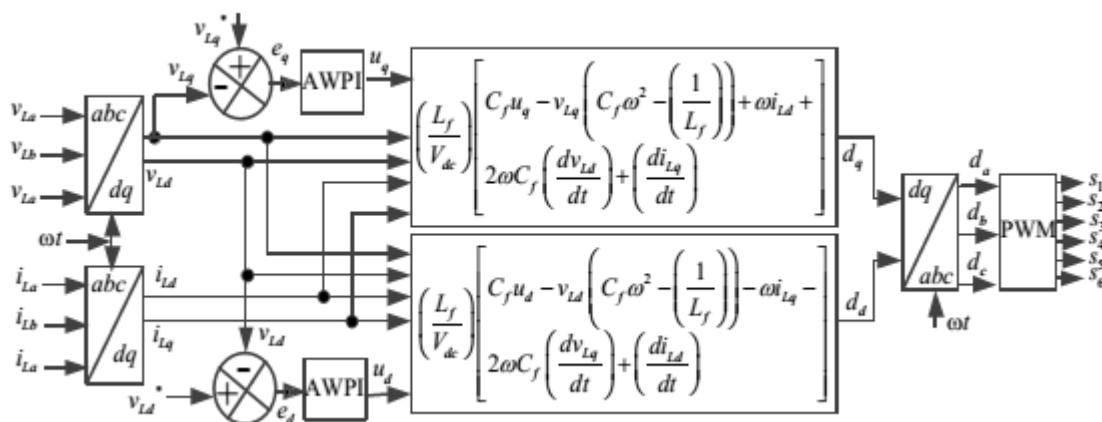


Figure 4: APC based Fuzzy in place of awPI controller for DC-AC interfacing inverter

Applying Park’s transformation to (60) and (61), one obtains the following expressions in d, q rotating frame as,

$$\begin{cases} (di_{invd} / dt) = (V_{dc} / L_f)d_d + i_{invq}\omega + v_{Ld} \\ (di_{invq} / dt) = (V_{dc} / L_f)d_q - i_{invd}\omega + v_{Lq} \end{cases} \tag{62}$$

$$\begin{cases} (dv_{Ld} / dt) = (1 / C_f)(i_{invd} - i_{Ld}) + \omega v_{Lq} \\ (dv_{Lq} / dt) = (1 / C_f)(i_{invq} - i_{Lq}) - \omega v_{Ld} \end{cases} \tag{63}$$

Replacing (62) in the derivative of (63), one gets the following expressions,

$$\begin{cases} C_f(d^2v_{Lq} / dt^2) = v_{Lq}(C_f\omega^2 - (1 / L_f)) - 2\omega C_f(dv_{Ld} / dt) + (V_{dc} / L_f)d_q - \omega i_{Ld} - (di_{Lq} / dt) \\ C_f(d^2v_{Ld} / dt^2) = v_{Ld}(C_f\omega^2 - (1 / L_f)) + 2C_f\omega(dv_{Lq} / dt) + (V_{dc} / L_f)d_d + \omega i_{Lq} - (di_{Ld} / dt) \end{cases} \tag{64}$$

where  $u_d$  and  $u_q$  denote new equivalent inputs, and  $\omega$  is pulsation, which is defined as,

$$\omega = 2\pi f_s \tag{65}$$

where  $f_s$  denotes the system frequency and is set equal to 60Hz.

From (64), one extracts the control laws  $d_d$  and  $d_q$  as,

$$\begin{cases} d_q = (L_f / V_{dc}) \left[ C_f u_q - v_{Lq} \left( C_f \omega^2 - \left( \frac{1}{L_f} \right) \right) + \omega i_{Ld} + 2\omega C_f \left( \frac{dv_{Ld}}{dt} \right) + \left( \frac{di_{Lq}}{dt} \right) \right] \\ d_d = (L_f / V_{dc}) \left[ C_f u_d - v_{Ld} \left( C_f \omega^2 - \left( \frac{1}{L_f} \right) \right) - \omega i_{Lq} - 2\omega C_f \left( \frac{dv_{Lq}}{dt} \right) + \left( \frac{di_{Ld}}{dt} \right) \right] \end{cases} \tag{66}$$

The dq-axis AC voltages  $v_{Ld}$  and  $v_{Lq}$  are controlled independently by acting upon the inputs  $u_d$  and  $u_q$ , respectively. However, the tracking controllers, are obtained as follows [32],

$$\begin{cases} u_q = (k\tau_c(\tau_i s + 1) / \tau_i(\tau_c s + 1))e_q + (1 / (\tau_c s + 1))u_{qmax} \\ u_d = (k\tau_c(\tau_i s + 1) / \tau_i(\tau_c s + 1))e_d + (1 / (\tau_c s + 1))u_{dmax} \end{cases} \tag{67}$$

where  $e_{d,q}$ ,  $v_{Ld,q}$ ,  $k$ ,  $\tau_i$ , and  $\tau_c$  denote the dq-axis AC voltage error, dq-axis AC voltages, proportional, integral feedback gain coefficients, respectively.

Fig. 5 shows the block diagram for fuzzy controller with feedback path control for d and q axis to avoid the saturation problem. The fuzzy controller model is based on time constants  $\tau_c$  and  $\tau_i$ , as well as, the gain  $k$ , which have a

visible effect on system performance when saturation occurs. Therefore, to get high performance, optimal gains

design is required. The selected optimal gain values are given in Table II of Appendix.

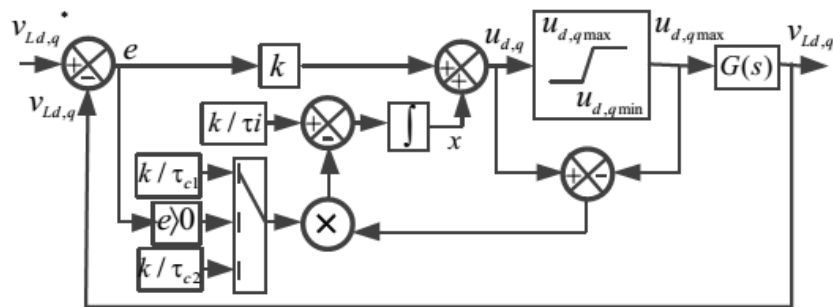


Figure 5: Block diagram of the fuzzy controller with feedback path control for d and q axis

#### 4. Simulation Results

Performance of the APC based fuzzy controller and improved P&O based SMC with boundary layer developed in this work are simulated under severe conditions using Matlab/Simulink and validated in real time using hardware prototype built in the laboratory.

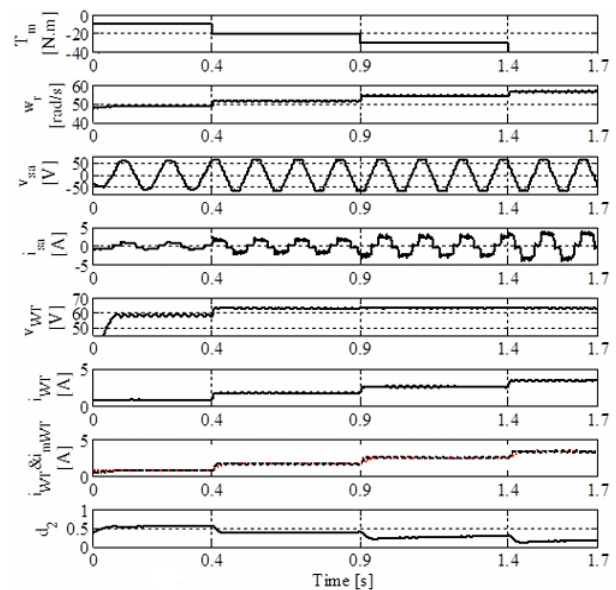
##### A. Performance of improved P&O based SMC with boundary layer for WT and SPVA under weather change

Fig.6 (a) shows the waveforms of the mechanical torque ( $T_m$ ), rotor speed of PMSM ( $\omega_r$ ), stator voltage ( $v_{sa}$ ) and current ( $i_{sa}$ ) of phase “a”, the output DC voltage ( $v_{WT}$ ), output DC current ( $i_{WT}$ ), inductor current ( $i_{WT} = i_{L2}$ ), the current reference ( $i_{mWT}$ ) and the desired control ( $d_2$ ). It is observed that  $i_{sa}$  and  $i_{WT}$  vary with variation of  $T_m$  developed by WT, the  $v_{sa}$  and  $v_{WT}$  vary slightly during variation of  $\omega_r$  compared to its rated values. It is clearly observed that  $i_{WT}$  varies with variation of  $\omega_r$ , with increments at  $t = 0.4$  s,  $0.9$  s and  $1.4$  s. The  $i_{WT}$  (which is equal to the  $i_{L2}$ ), follows its reference  $i_{mWT}$  during sudden variation and MPPT is achieved without measurement of  $\omega_r$  or wind speed. Furthermore, the control  $d_2$  remains within the defined range of variation even during transition and simultaneous operation of boost converter-1 and three-phase interfacing inverter, which confirms the robustness of the improved P&O method.

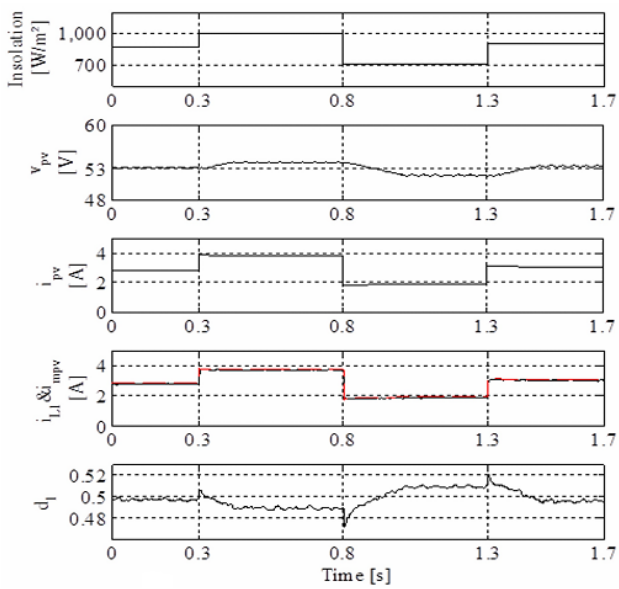
In Fig. 6 (b) the waveforms of the solar insolation, output PV voltage ( $v_{PV}$ ), output PV current ( $i_{PV}$ ), inductor current ( $i_{L1}$ ) and PV current reference ( $i_{mPV}$ ) and the control ( $d_1$ ), are presented. The solar insolation is increased at  $t=0.3$ s, decreased at  $t=0.8$ s and increased again at  $t=1.3$ s. It is observed that  $i_{L1}$  follows its reference during increase and decrease in solar insolation. MPPT from SPVA is achieved quickly without control divergence. However,  $d_1$  is not affected due to variation of solar insolation and simultaneously operation of boost converter-2, and the interfacing inverter. It is staying within the defined range during transient and steady state conditions. This confirms the robustness of the improved P&O based SMC with boundary layer.

##### B. Performance of the APC based fuzzy controller under different type of loads

Fig. 7 (a) shows the waveforms of the DC link voltage (V dc), which is equal to battery voltage ( $V_{bat}$ ), AC voltage ( $v_L$ ) and load current ( $i_L$ ), and the system frequency ( $f_s$ ) during: a) steady-state, b) sudden increased in linear load at  $t=0.1$ s, c) phase “a” load is switched ON between  $t=0.03$ s and  $t=0.13$ s, and d) presence of balanced and unbalanced nonlinear load. This test is performed under load and weather condition change. One can see clearly that APC based AWPI controller performs well during severe conditions, such as disconnected load in Fig.7 (b) between  $t=0$  s and  $t=0.1$ s and during presence of unbalance linear load in Fig.7 (c), as well as balanced and unbalanced nonlinear load in Fig.7 (d). It is observed in Figs.7 (a-d) that the AC voltage is regulated constant and sinusoidal with zero steady state error. It is demonstrated that APC performs well under different conditions. Furthermore it is proven that fuzzy controller perform well during transient and steady state without any saturation and control divergence. This confirms the robustness of the APC based on fuzzy controller.

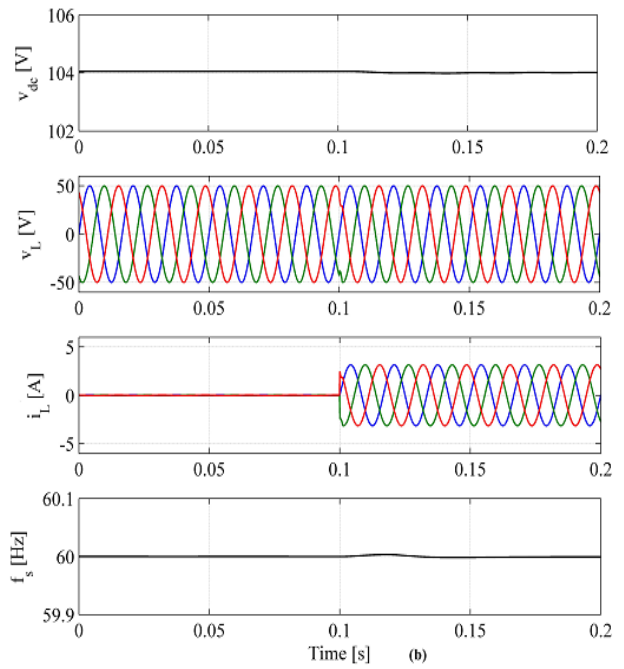


(a)

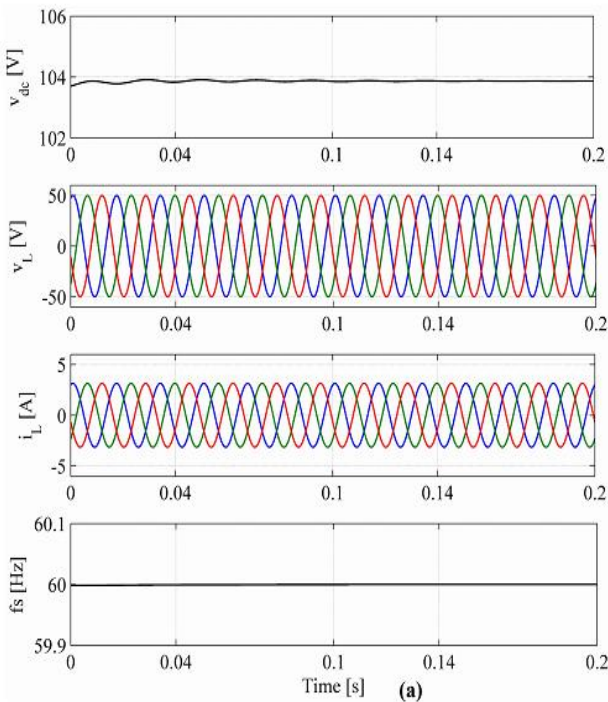


(b)

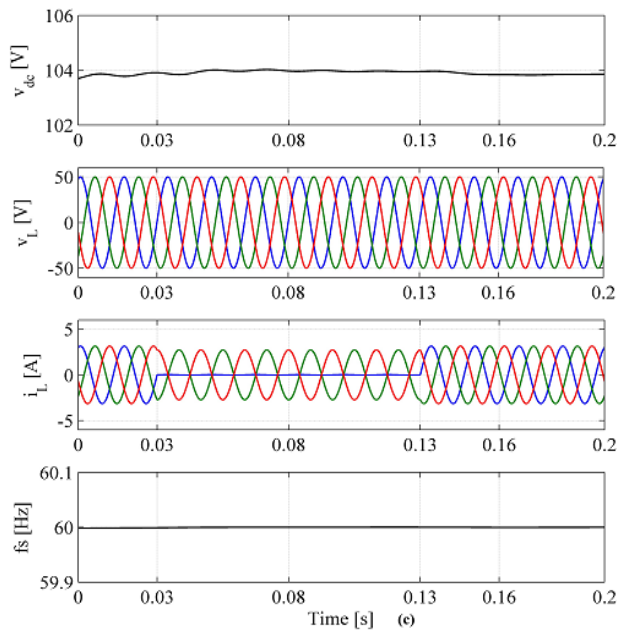
Figure 6: a) Obtained results of improved P&O based SMC with boundary layer WT side, and b) SPVA side.



(b)



(a)



(c)

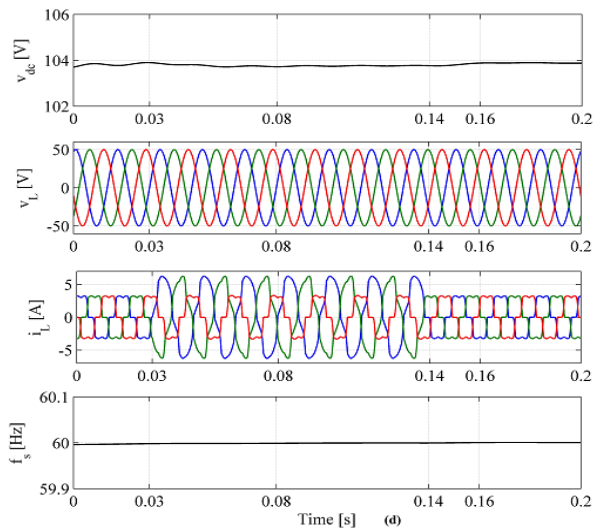


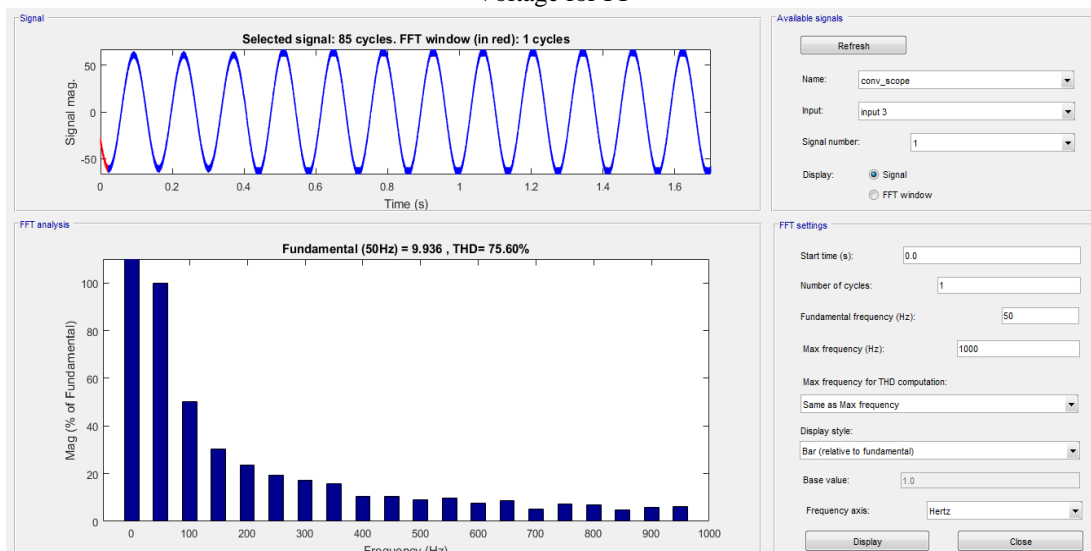
Figure 7: Performance of the APC based fuzzy controller under a) steady state, b) sudden increased of load at t=0.1s,

c) unbalance linear load, and d) balanced and unbalanced nonlinear load.

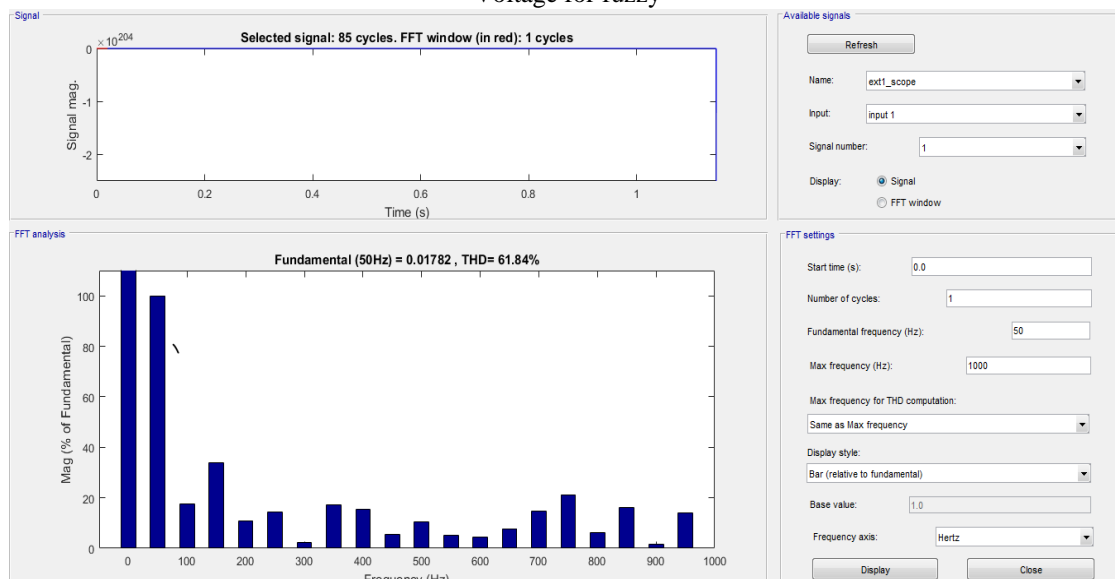
### 5. Conclusion

A wind-PV-battery based hybrid power generation system has been proposed for standalone application. Modeling, control design, and stability analysis have been presented in detail. Simulated performance of the system has been obtained with an improved P&O method for MPPT of SPVA and WT. For a multiple source power generation system, SMC with boundary layer is designed for improved performance under variable weather conditions. It has been demonstrated that the improved P&O based MPPT is more reliable and efficient during weather changes in presence of many power converters operated simultaneously. As contrasted and Anti-windup PI controller Fuzzy controller plays out the improvement in precision, acting time and waveform aggravations.

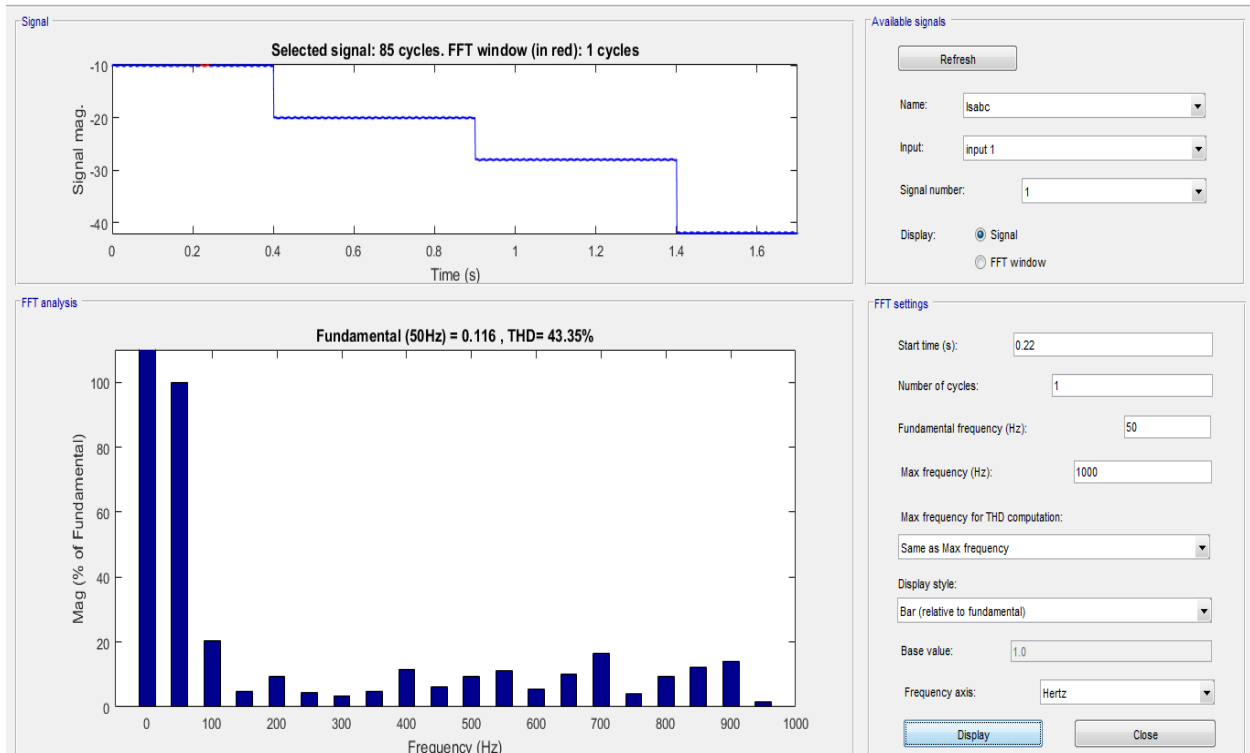
### THD values of HSPGS1 Voltage for PI



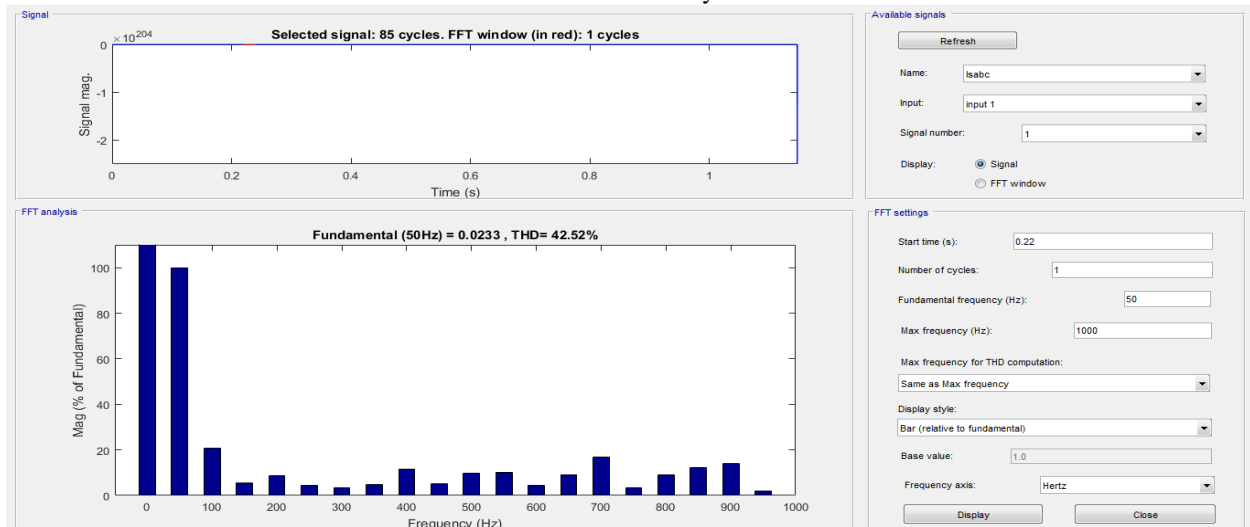
### Voltage for fuzzy



Current in PI



Current in fuzzy



The THD (total harmonic distortion) which represents the harmonic distortion of the waveforms is high for the PI controller and low for the fuzzy controller. The harmonics are decreasing in case of the fuzzy controller compared to PI controller. The following are the advantages of the fuzzy compared to PI

- 1) The harmonic distortions will be less
- 2) The steady state will be achieved in less time than PI
- 3) The settling time will be less in fuzzy and the response is increased
- 4) The overshoots will be minimized in case of fuzzy compared to PI.

References

- [1] D. Li and Z. Q. Zhu, "A Novel Integrated Power Quality Controller for Microgrid," IEEE Trans. Ind. Electr, vol. 62, no5, pp. 48-58, May 2015.
- [2] A. C. Luna, N. L. D. Aldana, M. Graells, J. C. Vasquez, and J. M. Guerrero, "Mixed-Integer-Linear-Programming based Energy Management System for Hybrid PV-wind-battery Microgrids: Modeling, Design and Experimental Verification," IEEE Trans. Power Electro.vol. 32, no4, pp. 2769-2783, April 2017.
- [3] M. A. G. d. Brito, L. Galotto, L. P. Sampaio, G. d. A. e. Melo, and C. A. Canesin, "Evaluation of the Main MPPT Techniques for Photovoltaic Applications," IEEE Trans. Ind. Electron.,vol. 60, no 3, pp.56-67, March 2013.
- [4] K. H. Kim, T. L. Van, D. C. Lee, S. H. Song, and E. H. Kim, "Maximum Output Power Tracking Control in

Variable-Speed Wind Turbine Systems Considering Rotor Inertial Power,” IEEE Trans. Ind. Electron., vol.60, no8, pp. 3207-3217, Aug. 2013

- [5] M. Rezkallah, S. K. Sharma, A. Chandra, B. Singh, and D. R. Rouse, “Lyapunov Function and Sliding Mode Control Approach for the SolarPV Grid Interface System,” IEEE Trans. Ind. Electron., vol. 64, no1, pp. 785-795, Jan. 2017